

Imperviousness Density Mapping Based on GIS-MCDA and High-Resolution Worldview-2 Imagery

Lovre Panda ^a

University of Zadar, Department of Geography, Trg kneza Višeslava 9, Zadar, Croatia

Keywords: WorldView-2, Imperviousness Density, GIS MCDA, LULC, NDVI, Slope, TWI, Urban Area, Zadar, Croatia.


Abstract: Accurate monitoring and extraction of impervious surfaces are essential for urban planning and sustainable environmental management. Increasing urbanization has led to a significant increase in the extent of impervious surfaces, which, along with climate change, are the leading cause of increasingly frequent flooding in urban areas. To prevent flooding disasters in urban areas, flood hazard and risk analyses must be carried out. An imperviousness density model is one of the most important criteria in such analyses. In this study, an imperviousness density model of the city of Zadar was created using GIS-MCDA and four criteria (LULC, NDVI, slope and TWI). The criteria were extracted from WorldView-2 (WV-2) imagery and linearly standardized using the Fuzzy logic approach. The Analytic Hierarchy Process (AHP) was used to determine the final model for imperviousness density. The model with a spatial resolution of 0.5 m, based on the WV-2 imagery turned out to be much more detailed than existing publicly available models, such as the Copernicus imperviousness density model, which is based on Sentinel-2 imagery with a spatial resolution of 10 m.

1 INTRODUCTION

The rapid growth of the world's population and increasing urbanization have led to a significant increase in the extent of impervious surfaces in urban areas (Duan et al., 2022) while decreasing the extent of forests, wetlands, green areas and bare soil (Xu, 2016). Impervious surfaces are man-made surfaces covered with materials such as asphalt or concrete that prevent the infiltration of water into the underground (Weng, 2012). In urban areas, this can include asphalted roads, sidewalks, parking lots, paved yards, airport runways, shipping ports, squares, cemeteries, etc. Also, a large portion of impervious surfaces in urban areas are buildings with roofs made of tile, concrete or sheet metal. Impervious surfaces have a great impact on the creation of urban heat islands and flood-prone areas (Fu et al., 2019). Furthermore, the increasing number of impervious surfaces can also disrupt the groundwater cycle and increase the risk of urban flooding (Brun and Band, 2000). To prevent flooding disasters in urban areas, flood hazard and risk analyses must be carried out. An imperviousness density model is one of the most important criteria in such analyses. Impervious

surface models are created in different ways, but generally, they can be divided into four main categories: (1) machine learning methods (Okujeni et al., 2018; Zhang et al., 2018), (2) spectral indices (Liu et al., 2013; Sun et al. 2015), (3) regression model (Okujeni et al., 2013; Ou et al., 2019), and (4) spectral mixture analysis (Herold et al., 2004; Yang and He, 2017). However, the methods are being improved every day and new methods are proposed for extracting impervious surfaces (Su et al., 2022). The input data is very important for the creation of a high-quality model. Data is collected from various multispectral sensors placed on a specific platform such as satellites, aircraft or drones. The choice of a platform and sensor affects the spatial, spectral, radiometric and temporal resolution, which in turn affects the output results (Aasen et al., 2018).

Multicriteria GIS decision analysis (GIS-MCDA) has not yet been used to create imperviousness density models. Various criteria such as land use – land cover model (LULC), vegetation indices or hydrological and geomorphological criteria can certainly be of great help in the detailed mapping of imperviousness. Publicly available imperviousness density models created by Copernicus, based on

^a <https://orcid.org/0000-0003-4549-4481>

Sentinel 2 imagery (URL1) are an excellent input for hydrological-hydraulic analysis based on models of lower spatial resolutions. However, for analyses based on higher spatial resolution models, it is necessary to create an imperviousness density model that follows the spatial resolutions of other high-resolution inputs.

The main goal of this research is to generate a GIS-MCDA imperviousness density model of Zadar using high-resolution WorldView-2 (WV-2) satellite imagery with a spatial resolution of 0.5 m.

1.1 Study Area

The study area is the City of Zadar located in the middle of the Croatian coast (Figure 1). Zadar is the fifth largest city in the Republic of Croatia and has gone through rapid urban growth in recent decades (Magaš, 1991; Graovac, 2004). This research is focused only on the mainland part of the City of Zadar, which in total covers 52.36 km² (Figure 1).

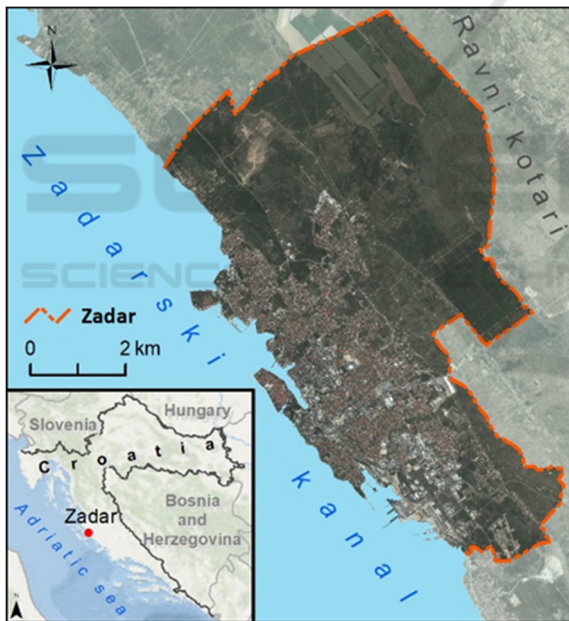


Figure 1: Geographical position of Zadar.

As a result of rapid urbanization and climate change, pluvial flooding caused by short-peak rainfall is becoming more frequent (Hallegatte et al., 2013; Woodruff et al., 2013). Of particular note is the major flood event on September 11, 2017, when a rain of great intensity in a short time (only 2 hours) caused extreme precipitation and flash floods. The rain of a slightly weaker intensity continued to fall throughout the morning and early afternoon and further worsened the situation. In 24 hours, a total of 285 mm of rain

fell in Zadar causing significant material damage (DHMZ, 2017).

2 METHODOLOGICAL FRAMEWORK AND DATA

The methodological framework is divided into several steps that include the acquisition and pre-processing of satellite imagery, the creation of criteria for the GIS-MCDA and the GIS-MCDA process itself (Figure 2).

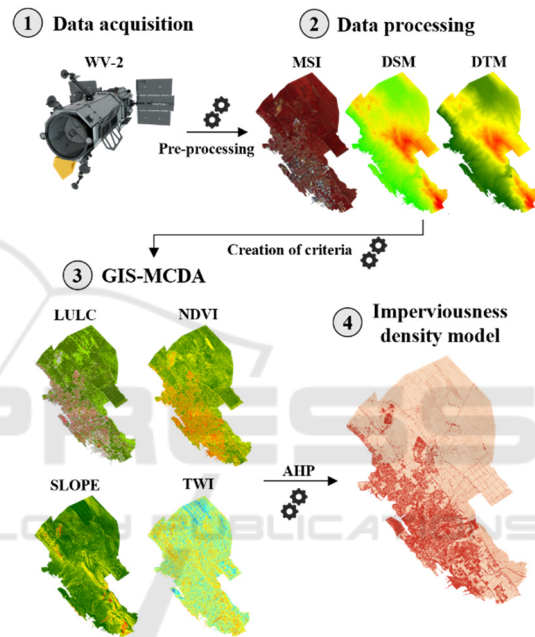


Figure 2: The methodological framework of the research.

2.1 Acquisition of WV-2 Satellite Imagery

Launched in October 2009, WV-2 is the first commercial satellite equipped with a high-resolution multispectral sensor with 8 spectral bands. The WV-2 satellite collects data in 8 different spectral bands and one panchromatic band. The eight multispectral bands (Coastal, Blue, Green, Yellow, Red, Red Edge, NIR1 and NIR2) have a spatial resolution of 2 m, while the panchromatic band has a spatial resolution of 0.5 m (DigitalGlobe, 2010a; Maxar, 2020).

Since the production of orthorectified multispectral image (MSI) and high-resolution digital terrain model (DTM) is planned for the wider area of the city of Zadar, it was decided to acquire ortho-ready stereo (OR2A) satellite WV-2 data. OR2A

satellite imagery is projected onto a constant elevation base calculated as the average terrain elevation within a given polygon. Therefore, OR2A satellite imagery is suitable for further processing and orthorectification of a custom high-resolution DTM (DigitalGlobe, 2010b).

2.2 Pre-processing of WV-2 MSI

Preprocessing of satellite imagery is crucial for the removal of various deformations and distortions in satellite images (Campbell and Wynne, 2011). Therefore, within this manuscript preprocessing has covered the following four steps:

2.2.1 Creation of a DSM

A digital surface model (DSM) of Zadar was created from the provided WV stereo images in the OrthoEngine 2018 extension of Geomatica 2018 software. The entire process of creating a DSM in the OrthoEngine extension can be divided into the following steps: (1) Selecting a mathematical model, (2) adding ground control (GCP) and check points (CP) required for stereo image orientation, (3) adding tie points (TP), (4) bundle adjustment, (5) creating of the epipolar image and (6) the automatic creation of the DSM.

In the first step, an optimal mathematical model was chosen for DSM extraction from the WV stereo imagery, where Optical Satellite modeling based on rational polynomial coefficients (RPC) and zero-order polynomial adjustment was chosen, as one the most commonly used mathematical models (Aguilar et al., 2013a; Goldbergs et al., 2019).

In the second step, a total of 35 GCPs and 12 CPs, collected with a real-time kinematic (RTK) GPS, were added (2) to correct errors caused by the application of RPC and to improve the overall georeferencing accuracy (Aguilar et al., 2013a; Goldbergs et al., 2019).

In the third step, a total of 264 TPs were automatically collected (3) using stereo imagery pixel correlation algorithms in Geomatica 2018 software.

In the fourth step, GCPs, TPs and the sensor geometry generated from the RPC coefficients were used for bundle adjustment (4) to calculate the exact position of the satellite at the moment of acquisition.

The fifth step includes the creation of an epipolar image (5), which represents a stereo pair of images, where both images are reprojected so that they have a common orientation and distribution along the common x-axis (URL2). The created epipolar image

is the basis for the process of automatically creating a DSM.

The final step of creating a DSM in the OrthoEngine extension of the Geomatica software is the automatic generation of a DSM (6) from the created epipolar image. The method of semi-global generation (Semi-global matching) of DSM was used in the process. To achieve the maximum possible spatial resolution of the created DSM, the pixel sampling interval was set to the value 1. Thus, the correlation of the stereo images and the creation of the DSM was performed with the maximum resolution of the images, enabling the generation of the high-resolution model (URL2).

2.2.2 Creation of a DTM

Unlike DSM, which represents the surface of the relief, natural (e.g. vegetation) and anthropogenic (e.g. residential buildings, roads, industrial facilities, etc.) surfaces located on the surface of the relief, a DTM only represents the surface of the relief (Šiljeg, 2013). Since slope is one of the criteria and an important criterion for the creation of the topographic wetness index model (TWI), it was necessary to create a DTM. The process of a DSM correction and filtering for the creation of the DTM can be generally divided into two steps: (1) Automatic correction of the DSM into the DTM and (2) the manual filtering of the remaining errors.

The automatic correction of the DSM into the DTM (1) was performed in the Geomatica 2018 software using the DSM2DTM algorithm, which enables the automatic filtering of the DSM according to the given user-defined parameters. The DSM2DTM algorithm automatically transforms the DSM into a DTM by applying a series of filtration steps that progressively remove anthropogenic and natural elements and smooth the final model by removing remaining irregularities, such as depressions and elevations, that do not represent relief surfaces.

After the automatic conversion of the DSM into a DTM, it was necessary to manually remove all remaining errors (2), resulting from the automatic filtering process. Errors in the created model occurred mainly in areas covered by water surfaces (e.g. the sea), where due to the uniformity of the surface, the software could not perform correlation and connection of pixels of the satellite imagery. Unlike artifacts on water surfaces, which include continuous parts of the model, the errors remaining after vegetation and anthropogenic objects were removed were individual, spatially heterogeneous errors that

could not be removed automatically. Therefore, error removal was performed manually using the DTM correction filter from the DEM editing extension of the Geomatica 2018 software.

2.2.3 Orthorectification of the WV-2 MSI

Orthorectification is one of the most important steps of satellite data pre-processing (Aguilar et al., 2013b), which is used to correct the geometry distortions of the data created during data acquisition (Belfiore and Parente, 2016). Orthorectification of the WV-2 imagery was performed using OrthoEngine 2018 software, based on the DSM previously created from the WV-2 stereo imagery. The process was performed only for one multispectral and one panchromatic image, where the representation of anthropogenic objects was better, e.g. less shadows and lower building distortions. This is especially the case with tall buildings such as skyscrapers or industrial plants. In addition to the DTM, available polygons of anthropogenic objects were also used for the orthorectification of multispectral and panchromatic images. Based on the available polygons, a more accurate orthorectification (true orthorectification) was performed.

2.2.4 Pan-Sharpening of WV-2 Imagery

Pan-sharpening of satellite imagery combines high-resolution panchromatic imagery with lower-resolution MSI, creating a unique MSI with a resolution equal to the resolution of the panchromatic image (Belfiore et al., 2016). There are many different methods for pan-sharpening of satellite images, which ultimately affect the appearance and quality of the sharpened images (Belfiore et al., 2016; Rajput et al., 2019). It should be noted that each sharpening method degrades the MSI input to some degree, primarily by deforming the shape or spectral values of the original image to improve the spatial resolution of the final image (Cheng and Chaapel, 2010). Although a special Hyperspherical Color Space (HCS) method (DigitalGlobe, 2010c) was developed to sharpen WV images, this method did not prove to be the best solution in the visual comparison of different sharpening algorithms. However, the PANSHARP2 algorithm from the Geomatica 2018 software was used to sharpen the WV-2 images, which caused significantly less distortion of the spectral values compared to the HCS algorithm and other algorithms tested.

2.3 Generating Criteria for the GIS-MCDA

A total of four criteria (LULC, NDVI, slope and TWI) generated from the WV-2 MSI and the DTM were used in the GIS-MCDA process.

The LULC model was created using the GEOBIA method. First, the WV-2 MSI was segmented using the Mean Shift method (Comaniciu and Meer, 2002). The spectral detail parameter was set to 15.5, the spatial detail was set to 15 and the minimum segment size was set to 20. The band sequence 8 4 1 (NIR2, Yellow, Coastal) is used, which allows different types of land cover to be viewed in different colors. This band combination can be used to quickly identify land use and land cover (URL3). Vegetation is in red, built-up areas are in blue, and changes in vegetation and structures are shown in different colors. A total of 1,200 samples were collected in six classes (water, asphalt/concrete/rock, buildings, low vegetation, forest, and soil). The segmented WV-2 image was then classified using the Support Vector Machine (SVM) algorithm (Aguilar et al., 2014; Lin et al., 2015; Wu et al., 2017; Mugiraneza et al., 2019). The created DSM was used as an additional parameter.

NDVI is a measure of the condition or health of vegetation in a certain area, determined based on the reflectance of certain spectral values (Maglione et al., 2014; Moody et al., 2014). Healthy vegetation reduces the susceptibility of a certain area to the process of soil erosion, as plants stabilize soil deposits with their roots and promote the infiltration of surface runoff into the soil (Arabameri et al., 2020). For this reason, high NDVI values, which represent healthy vegetation, also represent permeable areas. The NDVI model was created based on the spectral bands of the WV-2 MSI using the following formula (Maglione et al., 2014):

$$NDVI = \frac{NIR2 - Red}{NIR2 + Red} \quad (1)$$

The slope is a measure of the slope of each cell of the raster surface, i.e. the terrain surface (Gallant and Wilson, 2000). The Spatial Analyst extension of ArcGIS 10.1 software was used to create slope criteria using the Slope tool based on the Horn method (Horn, 1981). Slope affects the velocity of surface runoff, with velocity generally increasing as slope increases (Morgan, 2009). Therefore, the slope was used as one of the criteria because as the slope increases, the possibility of water retention and infiltration into the underground decreases.

The TWI is a hydrological measure of the potential wetness of a certain terrain, which defines

the tendency of a certain area to accumulate water (Różycka et al., 2017; Raduła et al., 2018). TWI enables the detection and analysis of different waterlogged areas (e.g. swamps, sinkholes, ravines, river valleys, etc.) characterized by high values of this index, and drier areas (e.g. steeper slopes and elevations) with low values of this index (Gallant and Wilson 2000). In this study, TWI was calculated using the Topographic Wetness Index tool from the Saga GIS extension for ArcGIS 10.1. The input data for the calculation of TWI were the slope and the size of the catchment area.

2.4 GIS-MCDA

Applied GIS-MCDA covered the following three steps: (1) standardization of criteria, (2) determination of weight coefficients (W_i) and (3) aggregation of standard criteria and W_i .

The developed six classes of LULC models were reclassified regarding the infiltration capacity of the substrate according to the NRCS methodology (USDA, 2017; Hong and Adler, 2008). Then, standardization was performed using the Fuzzy logic approach in ArcMap software. The Fuzzy Membership tool standardizes the raster criteria according to the chosen fuzzification algorithm on a scale of 0-1, where a value of 1 indicates a maximum membership strength that gradually decreases towards 0 (ESRI, 2023). The linear method was used and impervious classes received higher values.

The NDVI criterion was also linearly standardized with lower NDVI values representing impervious surfaces being assigned a higher value.

The slope criterion was also linearly reclassified so that higher slope values represent lower throughput.

The criterion TWI was linearly reclassified so that higher index values mean potentially higher throughput and lower index values mean lower throughput potential.

The Analytic Hierarchy Process (AHP) was used to determine the W_i required for the creation of the final imperviousness density model. The highest W_i was assigned to the LULC, which is the most important criterion in imperviousness density mapping. The NDVI criterion is the next in terms of importance, as it allows well distinction between permeable and impervious surfaces. The smallest W_i were assigned to the criteria of slope and TWI because their influence exists, but is not as significant as, for example, LULC. (Table 1). The CR was 0.1, which is 10% and is considered acceptable.

Table 1: AHP preference matrix and assigned W_i for the created criteria.

	LULC	NDVI	SLOPE	TWI	W_i
LULC	1	5	8	9	64.79
NDVI	0.2	1	6	7	24.64
SLOPE	0.125	0.167	1	2	6.33
TWI	0.111	0.143	0.5	1	4.24

In the final step, the GIS-MCDA model was created, based on the aggregation of standardized criteria and their W_i .

3 RESULTS AND DISCUSSION

Using the methodology GIS-MCDA and the Fuzzy logic approach to standardize the criteria, a model of imperviousness density was created. A total of four criteria were created and used in the further process (LULC, NDVI, slope and TWI).

The developed LULC model distinguished impervious surfaces very well compared to the WV-2 MSI. The most dominant LULC class within the study area is forest, while impervious classes (buildings, asphalt/concrete/rock) are mostly concentrated in urban coastal parts (Figure 3A).

The NDVI model best showed the difference between permeable surfaces, shown in shades of green, and less permeable and impervious surfaces, shown in shades of red (Figure 3B). Numerous researchers have used the NDVI and other indices derived from MSI in impervious surface extraction (Sun et al., 2015; Feng and Fan, 2019), and therefore this is certainly one of the more important criteria.

The slope criterion created on the DTM serves as a criterion that increases the degree of imperviousness on steeper slopes (Ansari et al., 2016). Within the research area, leveled and slightly sloping terrain prevails, which is why, if only this criterion is considered, most areas have a greater possibility of permeability. Steeper slopes comprise a very small part of the research area, which is mainly related to anthropogenic forms (quarry and waste dump) or natural slopes, and these areas are marked as less permeable (Figure 3C).

The criterion TWI distinguished areas that tend to accumulate water from the topographic basin. The areas that have a lower tendency to accumulate water, therefore, have a lower probability of water infiltration. TWI values within the research area are determined by the morphology of the relief, with elevated parts recording lower values of this index, which indicates less water accumulation (Figure 3D). On the other hand, the lower parts of the relief record

higher values of TWI, that is, they indicate a greater possibility of accumulating a significant amount of water. According to TWI, it is possible to distinguish two areas of water accumulation within the research area. The first area includes the coastal part including the center of the city of Zadar, and the second area the depression on the outskirts of the city.

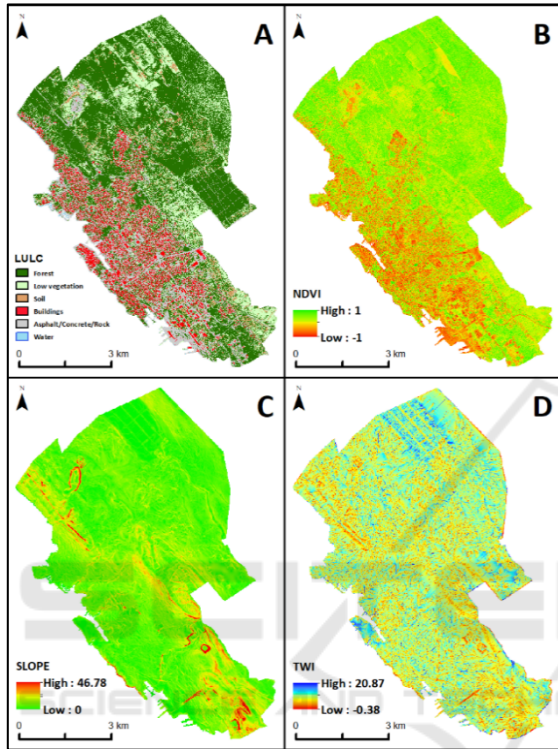


Figure 3: A) LULC; B) NDVI; C) Slope; D) TWI.

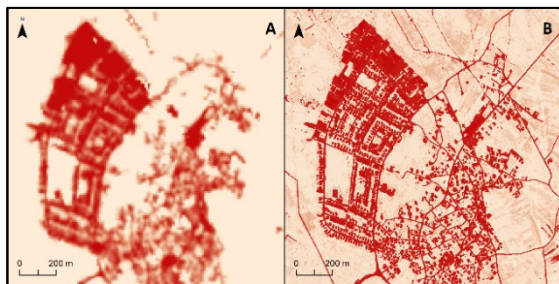


Figure 4: Imperviousness density based on A) Sentinel 2 MSI; B) WV-2 MSI.

The final imperviousness density model created from four linear standardized criteria shows that there are no completely permeable surfaces in Zadar (Figure 5). The lowest value for imperviousness of 0.23 was achieved by surfaces covered with forest, low vegetation and bare soil, while those covered with asphalt, concrete and rock have higher values.

Although green areas and bare soil are permeable surfaces, they have an infiltration capacity that is overloaded during extreme rainfall, when the substrate is oversaturated.

Comparing the imperviousness density model created with a spatial resolution of 0.5 m (Figure 4B), it is clear that it is significantly more detailed than the existing 10 m Copernicus model (Figure 4A). A quantitative comparison of these two models would not be relevant considering the large difference in spatial resolution. In the model created from the WV-2 imagery, objects are extracted in more detail, unlike the Copernicus model based on Sentinel 2.

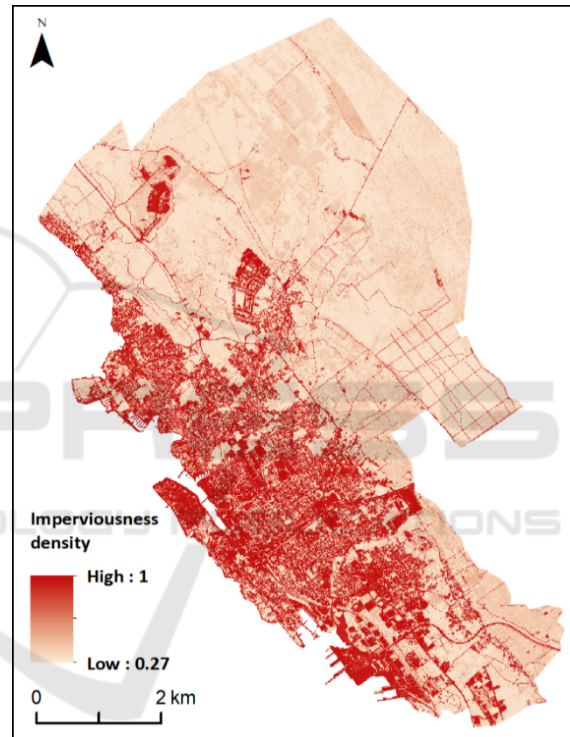


Figure 5: Imperviousness density model.

4 CONCLUSIONS

This paper describes a new approach to imperviousness density mapping using the GIS-MCDA method, based on four predisposing criteria. Depending on the quality of the input data, other criteria can also be considered, such as the drainage system or a more detailed LULC model. The existing Copernicus imperviousness density model is well suited for less detailed hydrological-hydraulic analyses. For more detailed analyses, it is necessary to create an imperviousness density model with higher spatial resolution. However, a more detailed

model requires a longer processing time, so a perfect balance should be found considering the purpose of the final model. The created model of imperviousness density in Zadar with a spatial resolution of 0.5 m is certainly the most detailed model of imperviousness of this area, which will serve as one of the spatial input data for hydrological-hydraulic 2D modeling in further studies. The same method will also be applied to create an imperviousness density model from data collected by a UAV multispectral camera with 10 bands and an aero-LiDAR system (ALS).

ACKNOWLEDGEMENTS

This research was produced as part of the Interreg STREAM (Strategic development of flood management) project, funded by the Italy-Croatia cross-border cooperation program 2014-2020 and the project UIP-2017-05-2694 financially supported by the Croatian Science Foundation.

REFERENCES

- Aasen, H., Honkavaara, E., Lucieer, A., & Zarco-Tejada, P. J. (2018). Quantitative remote sensing at ultra-high resolution with UAV spectroscopy: a review of sensor technology, measurement procedures, and data correction workflows. *Remote Sensing*, 10(7), 1091.
- Aguilar, M. A., Bianconi, F., Aguilar, F. J., & Fernández, I. (2014). Object-based greenhouse classification from GeoEye-1 and WorldView-2 stereo imagery. *Remote sensing*, 6(5), 3554-3582.
- Aguilar, M. A., del Mar Saldaña, M., & Aguilar, F. J. (2013a). Generation and quality assessment of stereo-extracted DSM from GeoEye-1 and WorldView-2 imagery. *IEEE Transactions on Geoscience and Remote Sensing*, 52(2), 1259-1271.
- Aguilar, M. A., del Mar Saldana, M., & Aguilar, F. J. (2013b). Assessing geometric accuracy of the orthorectification process from GeoEye-1 and WorldView-2 panchromatic images. *International Journal of Applied Earth Observation and Geoinformation*, 21, 427-435.
- Ansari, T. A., Katpatal, Y. B., & Vasudeo, A. D. (2016). Spatial evaluation of impacts of increase in impervious surface area on SCS-CN and runoff in Nagpur urban watersheds, India. *Arabian Journal of Geosciences*, 9(18), 1-15.
- Arabameri, A., Blaschke, T., Pradhan, B., Pourghasemi, H. R., Tiefenbacher, J. P., & Bui, D. T. (2020). Evaluation of recent advanced soft computing techniques for gully erosion susceptibility mapping: A comparative study. *Sensors*, 20(2), 335.
- Belfiore, O. R., & Parente, C. (2016). Comparison of different algorithms to orthorectify WorldView-2 satellite imagery. *Algorithms*, 9(4), 67.
- Belfiore, O. R., Meneghini, C., Parente, C., & Santamaria, R. (2016). Application of different Pan-sharpening methods on WorldView-3 images. *ARPN J. Eng. Appl. Sci*, 11(7).
- Brun, S. E., & Band, L. E. (2000). Simulating runoff behavior in an urbanizing watershed. *Computers, environment and urban systems*, 24(1), 5-22.
- Campbell, J. B., & Wynne, R. H. (2011). *Introduction to remote sensing*. Guilford Press.
- Cheng, P., & Chaapel, C. (2010). Pan-sharpening and geometric correction: worldview-2 satellite. *GeoInformatics*, 13(4), 30.
- Comaniciu, D., & Meer, P. (2002). Mean shift: A robust approach toward feature space analysis. *IEEE Transactions on pattern analysis and machine intelligence*, 24(5), 603-619.
- DHMZ - Državni hidrometeorološki zavod (2017). Available from: https://meteo.hr/objave_najave_nat_jecaji.php?section=onn¶m=objave&el=pricipcenj_a&daj=pr12092017 (Accessed on 17 November 2022).
- DigitalGlobe, Inc. (2010a): The Benefits of the 8 Spectral Bands of WorldView-2, <https://docslib.org/doc/5291751/the-benefits-of-the-eight-spectral-bands-of-worldview-2> (Accessed on 19 November 2022).
- DigitalGlobe, Inc. (2010b): DigitalGlobe Core Imagery Products Guide, https://lps16.esa.int/posterfiles/paper1213/%5bRD12%5d_digitalglobe-core-imagery-products-guide.pdf (Accessed on 20 November 2022).
- DigitalGlobe, Inc. (2010c) - WorldView-2 Imagery Basics and Erdas Imagine, <https://fddocuments.net/document/worldview2-basics-and-erdas-imagine.html?page=1> (Accessed on 22 November 2022).
- Duan, C., Zhang, J., Chen, Y., Lang, Q., Zhang, Y., Wu, C., & Zhang, Z. (2022). Comprehensive Risk Assessment of Urban Waterlogging Disaster Based on MCDA-GIS Integration: The Case Study of Changchun, China. *Remote Sensing*, 14(13), 3101.
- ESRI (2023). *Fuzzy Membership (Spatial Analyst) — ArcMap | Documentation* (n.d.). Available from: <https://desktop.arcgis.com/en/arcmap/latest/tools/spatial-analyst-toolbox/fuzzy-membership.htm> (Accessed on 24 February 2023).
- Feng, S., & Fan, F. (2019). A hierarchical extraction method of impervious surface based on NDVI thresholding integrated with multispectral and high-resolution remote sensing imageries. *Ieee Journal of Selected Topics in Applied Earth Observations and Remote Sensing*, 12(5), 1461-1470.
- Fu, Y., Liu, K., Shen, Z., Deng, J., Gan, M., ... & Wang, K. (2019). Mapping impervious surfaces in town-rural transition belts using China's GF-2 imagery and object-based deep CNNs. *Remote Sensing*, 11(3), 280.
- Gallant, J. C., & Wilson, J. P. (2000). *Terrain analysis: principles and applications* (Vol. 538). New York: John Wiley & Sons.
- Goldbergs, G., Maier, S. W., Levick, S. R., & Edwards, A. (2019). Limitations of high resolution satellite stereo imagery for estimating canopy height in Australian tropical savannas. *International Journal of Applied Earth Observation and Geoinformation*, 75, 83-95.
- Graovac, V. (2004). Populacijski razvoj Zadra. *Geoadria*, 9(1), 51-72.

- Hallegatte, S., Green, C., Nicholls, R. J., & Corfee-Morlot, J. (2013). Future flood losses in major coastal cities. *Nature climate change*, 3(9), 802-806.
- Herold, M., Roberts, D. A., Gardner, M. E., & Dennison, P. E. (2004). Spectrometry for urban area remote sensing—Development and analysis of a spectral library from 350 to 2400 nm. *Remote sensing of environment*, 91(3-4), 304-319.
- Hong, Y., & Adler, R. F. (2008). Estimation of global SCS curve numbers using satellite remote sensing and geospatial data. *International Journal of Remote Sensing*, 29(2), 471-477.
- Horn, B. K. (1981). Hill shading and the reflectance map. *Proceedings of the IEEE*, 69(1), 14-47.
- Lin, C., Wu, C. C., Tsogt, K., Ouyang, Y. C., & Chang, C. I. (2015). Effects of atmospheric correction and pansharpening on LULC classification accuracy using WorldView-2 imagery. *Information Processing in Agriculture*, 2(1), 25-36.
- Liu, C., Shao, Z., Chen, M., & Luo, H. (2013). MNDISI: A multi-source composition index for impervious surface area estimation at the individual city scale. *Remote sensing letters*, 4(8), 803-812.
- Magaš, D. (1991). Neke promeje u gradskim naseljima zadarske regije u razdoblju 1857.-1971. godine. *Radovi Zavoda za povijesne znanosti HAZU u Zadru*, (33), 239-258.
- Maglione, P., Parente, C., & Vallario, A. (2014). Coastline extraction using high-resolution WorldView-2 satellite imagery. *European Journal of Remote Sensing*, 47(1), 685-699.
- Maxar (2020): Worldview-2. Datasheet. (Accessed on 19 November 2022).
- Moody, D. I., Brumby, S. P., Rowland, J. C., Altmann, G. L., & Larson, A. E. (2014, October). Change detection and classification of land cover in multispectral satellite imagery using clustering of sparse approximations (CoSA) over learned feature dictionaries. In *2014 IEEE Applied Imagery Pattern Recognition Workshop (AIPR)* (pp. 1-10). IEEE.
- Morgan, R. P. C. (2009). *Soil erosion and conservation*. John Wiley & Sons.
- Mugiraneza, T., Nascetti, A., & Ban, Y. (2019). WorldView-2 data for hierarchical object-based urban land cover classification in Kigali: integrating rule-based approach with urban density and greenness indices. *Remote Sensing*, 11(18), 2128.
- Okujeni, A., Canters, F., Cooper, S. D., Degerickx, J., Heiden, U., Hostert, P., ... & van der Linden, S. (2018). Generalizing machine learning regression models using multi-site spectral libraries for mapping vegetation-impervious-soil fractions across multiple cities. *Remote sensing of environment*, 216, 482-496.
- Raduła, M. W., Szymura, T. H., & Szymura, M. (2018). Topographic wetness index explains soil moisture better than bioindication with Ellenberg's indicator values. *Ecological Indicators*, 85, 172-179.
- Rajput, U. K., Ghosh, S. K., & Kumar, A. (2016). Multi-sensor satellite pan-sharpening based on IHS and Window Pseudo Wigner distribution integrated approach: Application to WorldView-2 imagery. *International Journal of Image and Data Fusion*, 7(2), 119-147.
- Różycka, M., Migoń, P., & Michniewicz, A. (2017). Topographic Wetness Index and Terrain Ruggedness Index in geomorphic characterisation of landslide terrains, on examples from the Sudetes, SW Poland. *Zeitschrift für geomorphologie, Supplementary issues*, 61(2), 61-80.
- Šiljeg, A. (2013). *Digitalni model reljefa u analizi geomorfometrijskih parametara—primjer PP Vransko jezero* (Doctoral dissertation, Doktorski rad, PMF, Sveučilište u Zagrebu).
- Su, S., Tian, J., Dong, X., Tian, Q., Wang, N., & Xi, Y. (2022). An impervious surface spectral index on multispectral imagery using visible and Near-Infrared bands. *Remote Sensing*, 14(14), 3391.
- Su, S., Tian, J., Dong, X., Tian, Q., Wang, N., & Xi, Y. (2022). An impervious surface spectral index on multispectral imagery using visible and Near-Infrared bands. *Remote Sensing*, 14(14), 3391.
- Sun, G., Chen, X., Jia, X., Yao, Y., & Wang, Z. (2015). Combinational build-up index (CBI) for effective impervious surface mapping in urban areas. *IEEE Journal of selected topics in applied earth observations and remote sensing*, 9(5), 2081-2092.
- URL1: Imperviousness density 2018. <https://land.copernicus.eu/pan-european/high-resolution-layers/imperviousness/status-maps/imperviousness-density-2018?tab=metadata> (Accessed on 17 November 2022).
- URL2: https://catalyst.earth/catalyst-system-files/help/COMON/concepts/DEM_buildfromstereo.html (Accessed on 3 December 2022).
- URL3: <https://studylib.net/doc/7954755/worldview--2-band-combinations---c-agg> (Accessed on 20 December 2022).
- USDA (2017): Part 630 Hydrology: National Engineering Handbook, Chapter 9: Hydrological Soil-Cover Complexes.
- Weng, Q. (2012). Remote sensing of impervious surfaces in the urban areas: Requirements, methods, and trends. *Remote Sensing of Environment*, 117, 34-49.
- Woodruff, J. D., Irish, J. L., & Camargo, S. J. (2013). Coastal flooding by tropical cyclones and sea-level rise. *Nature*, 504(7478), 44-52.
- Wu, Q., Zhong, R., Zhao, W., Fu, H., & Song, K. (2017). A comparison of pixel-based decision tree and object-based Support Vector Machine methods for land-cover classification based on aerial images and airborne lidar data. *International Journal of Remote Sensing*, 38(23), 7176-7195.
- Xu, J., Zhao, Y., Zhong, K., Ruan, H., & Liu, X. (2016). Coupling modified linear spectral mixture analysis and soil conservation service curve number models to simulate surface runoff: application to the main urban area of Guangzhou, China. *Water*, 8(12), 550.
- Yang, J., & He, Y. (2017). Automated mapping of impervious surfaces in urban and suburban areas: Linear spectral unmixing of high spatial resolution imagery. *International Journal of Applied Earth Observation and Geoinformation*, 54, 53-64.
- Zhang, L., Zhang, M., & Yao, Y. (2018). Mapping seasonal impervious surface dynamics in Wuhan urban agglomeration, China from 2000 to 2016. *International journal of applied earth observation and geoinformation*, 70, 51-61.